Paper: ASAT-14-230-AE

14th International Conference on
AEROSPACE SCIENCES & AVIATION TECHNOLOGY,
ASAT - 14 – May 24 - 26, 2011, Email: asat@mtc.edu.eg
Military Technical College, Kobry Elkobbah, Cairo, Egypt
Tel: +(202) 24025292 –24036138, Fax: +(202) 22621908

Aerothermodynamics of Spiked Bodies: Part II

M.Y.M. Ahmed*, N. Qin†

Abstract: The two main design objectives namely, reducing the drag and reducing the aeroheating can be satisfied using the spikes and aerodisks. This field of aerodynamics has gained much interest over the years and is still attracting the researchers' interest. The target of this study is to illustrate these contributions. In the first part of this study, the aerothermodynamic characteristics of spiked bodies are discussed and the previous studies are illustrated. In this part, the recent contributions of the authors are presented and a number of future research areas are proposed.

I. Introduction

The hypersonic vehicles, which commonly have blunt shapes, are exposed to extreme drag and aeroheating levels. These unwanted effects can be alleviated by altering the flow pattern around the hypersonic vehicle using a variety of techniques. One of the simplest techniques is to attach a spike, a thin cylinder, at the stagnation point of the vehicle's nose. Adding a larger disk at the spike's tip, an aerodisk, can improve the spike as a drag and aeroheating reduction device. This simple alternation in the design of hypersonic vehicles generates a flowfield full of interesting details. This field has been, and still is, attractive to the aerodynamicists since 1947. In the first part of the present study [1], a survey of the huge body of experimental and numerical studies in this field are discussed and a number of "gaps" are addressed. The objective of the present paper is to introduce the contributions of the authors in this field. The paper finalizes with some recommendations for future studies.

II. Recent Contributions

The authors conducted a research on the spiked hypersonic vehicles using numerical simulation techniques [2]. The commercial CFD code, Fluent [3], was implemented in this research as the flow solver. The ultimate objective of the research was to find the optimum design of such vehicles for both minimum drag and aeroheating effects. The case study is a forebody of a blunt hypersonic vehicle flying with a Mach 6, zero incidence, and at an altitude of 60 Km in a standard atmosphere. In the context of this research, a thorough investigation of the aerodynamic characteristics was done and a number of new findings were revealed. In the present section, these findings are illustrated first. The results of the design optimization are discussed next.

* Egyptian Armed Forces, Egypt.
† Professor of Aerodynamics, Department of Mechanical Engineering, University of Sheffield, Sheffield, UK.

A. Investigation of the Aerothermodynamic Characteristics of Spiked Blunt Bodies

The investigation of the aerothermodynamic characteristics is conducted on a model of a hemispherical shape of a unit diameter, $D=1$, representing the forebody of the hypersonic vehicle. A spike of a variable length and a diameter of $d=0.05D$ is used and is equipped with a hemispherical aerodisk of a variable diameter. The spike length and the aerodisk diameter are varied such that the overall length of the spike-aerodisk assembly ranges from $0.5D$ to $2.5D$ and the aerodisk diameter ranges from 0 to $0.4D$ with a step 0.05. An aerodisk of zero diameter corresponds to a sharp-pointed spike whereas a diameter of $0.05D$ corresponds to a plain spike with a rounded tip. A total of 45 models were investigated. The geometry of the model is shown in Fig. 1.

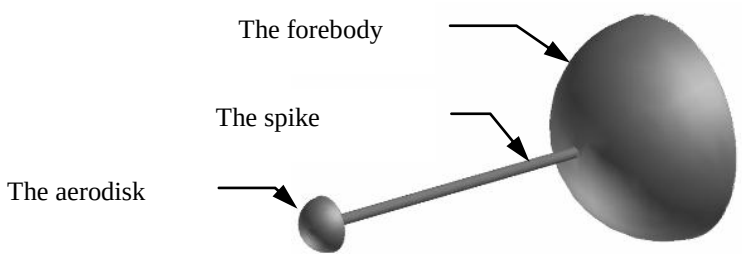

Figure 1 Geometry of the test model

The numerical simulation is conducted on an axisymmetric computational domain which is discretized into a structured grid using Gambit [4]. The sensitivity of the numerical solution to the grid resolution is studied. The validity of the numerical simulation scheme to this type of problems is addressed by comparing it with the experimental results of Crawford [5], Gnemmi et al. [6], and Kalimuthu et al. [7]. Both the grid sensitivity checks and validation tests are successful and show good results [2].

1. Mechanism of drag reduction, the effective body approach

The drag reduction experienced by spiked blunt bodies is commonly explained by the size of the recirculation zone which screens a considerable portion of the forebody [7-9]. Increasing the spike length causes the reattachment point to move further downstream along the forebody surface, the recirculation zone to expand covering a larger area of the forebody. In addition, the strength of the reattachment shock decreases as the reattachment point moves further towards the forebody shoulder (as a consequence of increasing the spike length). Hence, the surface pressure at the reattachment point is reduced. Overall, the drag is further reduced as the spike length increases. This explanation was widely adopted and was found to sufficiently explain the performance of spiked bodies. However, this explanation fails to address a number of phenomena associated with sharp-pointed spikes. Figure 2 illustrates the pressure variation along the spike surface and forebody surface for three models with sharp-pointed spikes. The horizontal axis in Fig. 2a represents the normalized distance measured from the conical tip shoulder whereas in Fig. 2b represents the angle from the model axis measured in the clockwise direction. In both figures, the local pressure is normalized with respect to the stagnation pressure of the unspiked body at the same freestream conditions, P_{ref}.

Firstly, increasing the spike length reduces the flow pressure *everywhere* and not only at the reattachment point. Secondly, the slight shift of the reattachment point seems insufficient to explain the significant reduction in the peak pressure. The concept of the effective body is implemented by the authors [10] to explain more accurately the mechanism of drag reduction in spiked bodies. In fact, the concept of the effective body is well-established in the field of

spiked bodies aerodynamics . It was first addressed by Alexander [11] and simply states that the spiked blunt body is effectively transformed into a more slender body due to the generation of the shear layer. For sharp-pointed bodies, Mair [12] argued that the shape of the recirculation zone was nearly conical and hence the flow outside the shear layer was very similar to a conical flow. He confirmed this explanation by comparing the inclination angle of separation shock with that ahead of a conical body having the same deflection as the shear layer.

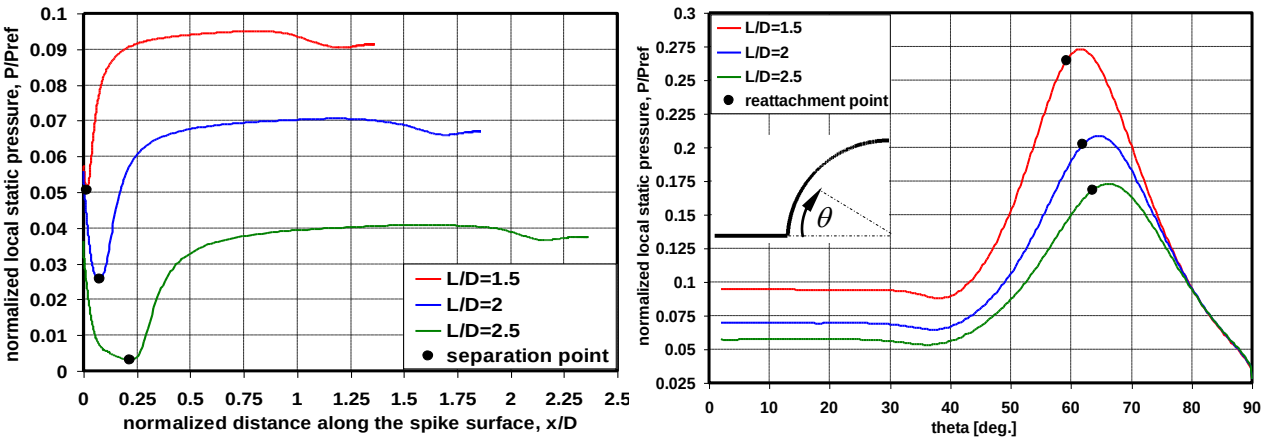

(a) along the spike surface **(b) along the forebody surface**

Figure 2 Surface pressure variation on three different models with pointed spikes

These angles were found to be in a close similarity. This hypothesis was supported by Crawford [5], Yamauchi et al. [9], and was recently confirmed quantitatively by Humieres and Stollery [13].

However, defining the effective body by the shear layer is not precise. This is because the thickness of the shear layer increases significantly with distance from the separation point [14]. In addition, at reattachment, part of the streamlines constituting the shear layer continues moving past the reattachment zone and merges with the flow downstream of the reattachment shock whereas others are reversed into the recirculation zone. The streamline that separates the "escaping" and "reversing" streamlines was defined by Chapman [14] as the dividing streamline. Wood [15] emphasized that, at equilibrium, the dividing streamline links the separation and reattachment stagnation points. In addition, it was shown [16] that the stability of this streamline dictates the overall stability of the flowfield. Figure 3 illustrates more details about the dividing streamline of a model with a sharp-pointed spike ($L/D=2$). Details at the reattachment point are shown on the right.

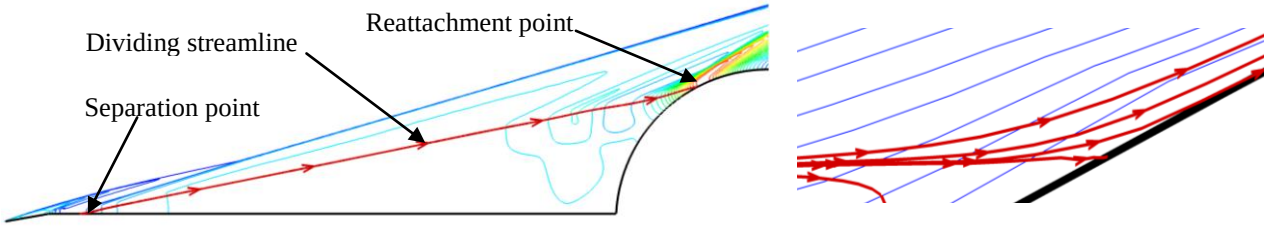

(a) **(b)**

Figure 3 Details of the dividing streamline

The pressure contours in Fig. 3a show that the locations of both separation and reattachment shocks are associated with both ends of the dividing streamline. The dividing streamline is the only streamline in the shear layer that completely stagnates on the body surface at the reattachment point as shown in Fig. 3b. Hence, we find it more accurate to use the dividing streamline rather than the shear layer to define the outer profile of the effective body. To validate this hypothesis, the dividing streamlines for three models with pointed spikes namely, with $L/D=1.5$, 2, and 2.5 are investigated. The inclination angles of dividing streamline and separation shock are compared with the theoretical analysis of supersonic flow around conical bodies [17] in Fig. 4. The comparison shows good agreement of the hypothesis with the theoretical relations.

It is clear from Fig.4 that increasing the spike length yields a more slender effective body (smaller θ). Here, the effective body is outlined by the dividing streamline along the shear layer and the physical body elsewhere. The form of the effective body dictates the pressure field in two ways namely, the inclination of the separation shock and the flow expansion ahead of separation. Firstly, the inclination of the dividing streamline governs the strength of the separation shock and, consequently, the entire pressure field downstream of separation. Secondly, the existence of an expansion fan ahead of separation further reduces the downstream pressure field which is indicated by the initial pressure drop on the spike, Fig. 2a. The extent of the expansion fan is dictated by the location of the separation point. Overall, increasing the spike length yields a further reduction in the pressure over the whole body surface including the reattachment point.

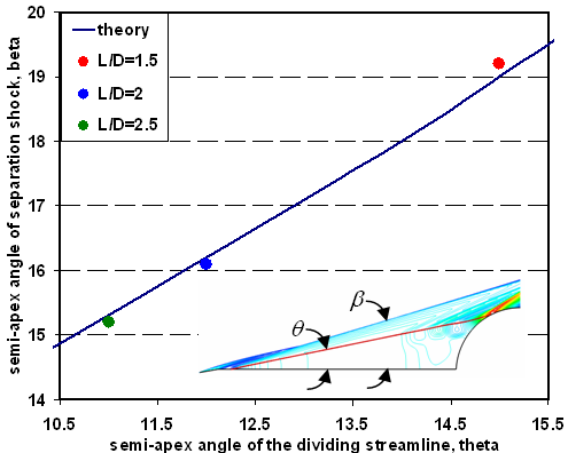

Figure 4 Inclination of the dividing streamlines and separation shocks in models with pointed spikes

The mechanism of drag reduction using aerodisks, their relative superiority, and the further drag reduction achieved by increasing their sizes are not clear from the current explanation and the previous investigations so far. Figure 5a illustrates the variation of local pressure along the forebody of four models having a spike length of $L/D=1.5$ and different aerodisk sizes. For comparison, the corresponding pressure distribution for a model with a pointed spike of the same length is also plotted. Figures 5b-e shows the shapes of the corresponding effective body as outlined by the dividing streamline.

In addition to the pressure reduction as the aerodisk size increases, two other phenomena can be addressed. Firstly, in the model with $d/D=0.4$, the surface pressure is further reduced despite that the reattachment point is shifted slightly towards the spike root. Secondly, a pressure reduction is achieved on the model with the sharp-pointed spike ($d/D=0.0$) simply

by rounding the spike tip ($d/D=0.05$). The hypothesis of the effective body based on the dividing streamline is employed for the explanation of drag reduction mechanism in models with aerodisks. Increasing the aerodisk size pushes the separation point (which is located at the aerodisk shoulder) further away from the forebody axis yielding a more slender effective body. By virtue of the flow expansion downstream of separation, the forebody is not affected by the strength of the foreshock ahead of the aerodisk. Moreover, it can be deduced that the size of the expansion fan (and hence the downstream pressure drop) increases with the aerodisk size since the dividing streamline inclination decreases at the separation point. In the model with $d/D=0.4$, the slenderness of the effective body and the size of the expansion fan yield a further reduction in the pressure field around the entire body despite that the reattachment point is closer to the spike root.

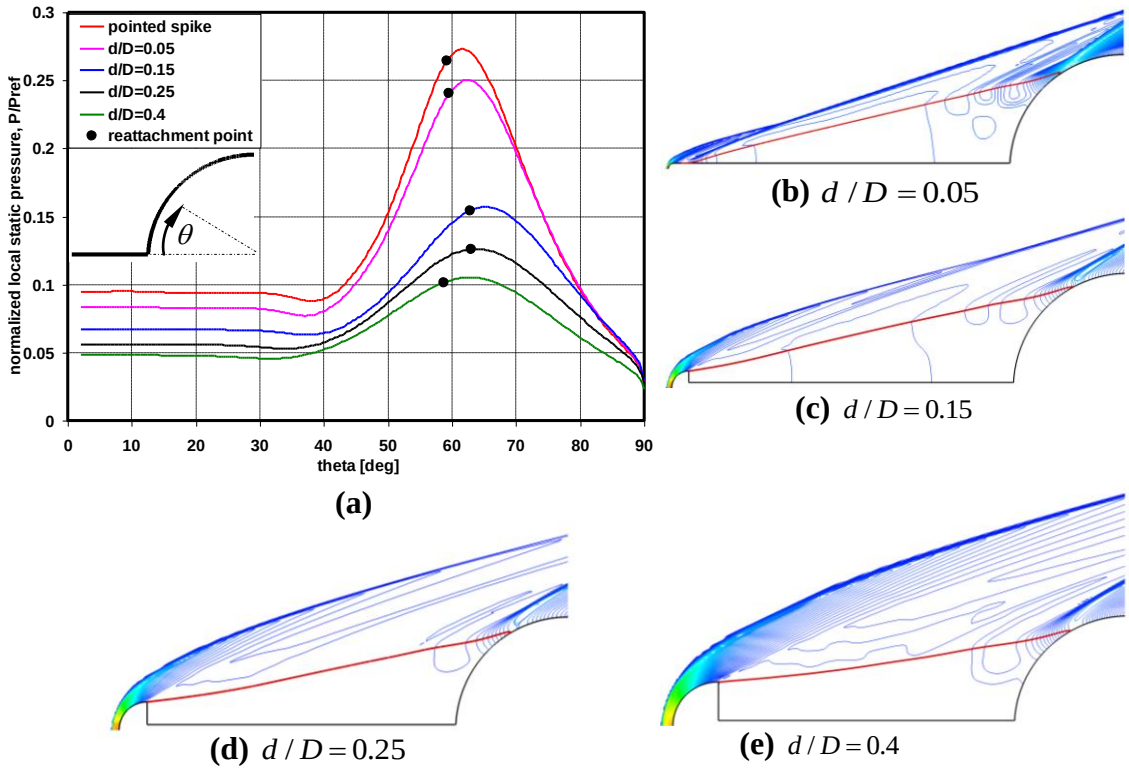

Figure 5 Impact of the aerodisk size on the pressure field and the effective body shape

The further pressure reduction gained by rounding the spike tip, $d/D=0.05$, compared with the sharp-pointed spike by the early separation of the dividing streamline and the wider expansion fan downstream of separation. These two aspects are depicted from Fig. 6. The combined effect of larger expansion and more slender effective body eventually reduces the whole pressure filed.

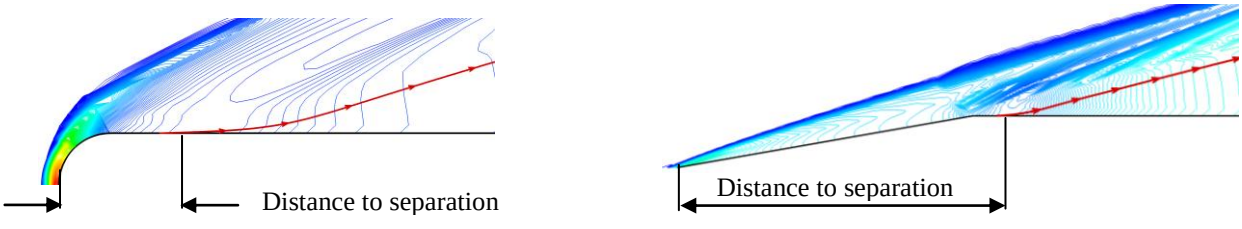

Figure 6 Impact of rounding the spike tip on the flow details at separation

2. Factors governing the effective body shape:

In models having spikes with pointed ($d/D=0.0$) or rounded ($d/D=0.05$) tips, the dividing streamline is almost a straight line linking the separation and reattachment points. Consequently, the effective body associated with these models has a conical shape, Fig. 7a and b. In these models, the location of separation point is governed by the adverse pressure gradient caused by the vicinity of the blunt forebody.

In contrast, in the models with aerodisks ($d/D>0.05$), the shear layer separates at the aerodisk shoulder. According to the spike length and aerodisk diameter, the shear layer may propagate directly towards the forebody or have a more curved profile. Hence, the shape of the effective body varies from one model to the other, Fig. 7c and d. The factors dictating the geometry of the effective body are explained here.

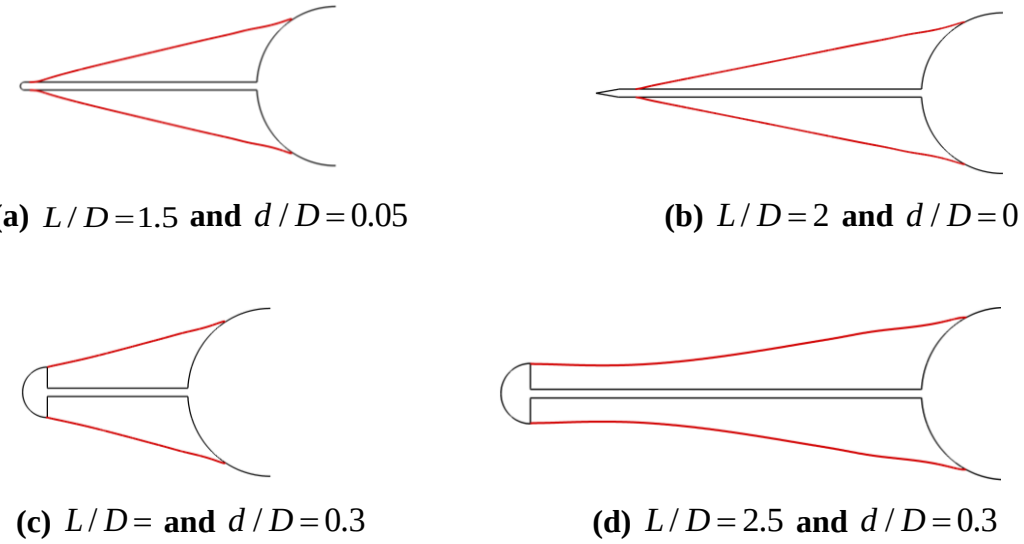

(a) $L/D=1.5$ **and** $d/D=0.05$ **(b)** $L/D=2$ **and** $d/D=0$

(c) $L/D=$ **and** $d/D=0.3$ **(d)** $L/D=2.5$ **and** $d/D=0.3$

Figure 7 Geometry of the effective body for four different models

Chapman [14] suggested that the parameter which dictates the flow pressure inside the recirculation zone and, hence, its size is the total pressure along the dividing streamline in the vicinity of reattachment zone. He argued that, for a stable reattachment, the pressure inside the recirculation zone is such that its corresponding total value is equal to the peak static reattachment pressure. The latter is, in turn, dictated by the flow turning angle at reattachment. Based on this argument, Kenworthy [16] introduced the "energetic shear layer" concept as the criterion for the oscillation mode around spiked flat cylindrical models. This approach was confirmed numerically by Feszty et al. [18]. Here, an attempt is made to extend and combine these hypotheses. The assumption is that, at equilibrium, the shape of the effective body is dictated by the energy level of the dividing streamline immediately downstream of the separation point. The dividing streamline that possesses high energy level (in terms of total pressure) manages to proceed directly to the reattachment point on the forebody surface. On the other hand, the dividing streamline that has low pressure (and, consequently, low energy) gets closer to the spike and even reattaches to it. Hence, depending on the spike length and aerodisk size, local values of Mach number and pressure attain certain values and their combination determines the energy level in the dividing streamline and eventually dictates the outlines of the effective body. To validate this assumption, the dividing streamline of the models having the same spike length ($L/D=2.5$) are investigated. Figures 8a and b illustrate the evolution of the shape and total pressure along the dividing streamline immediately after separation from the aerodisk shoulder, respectively.

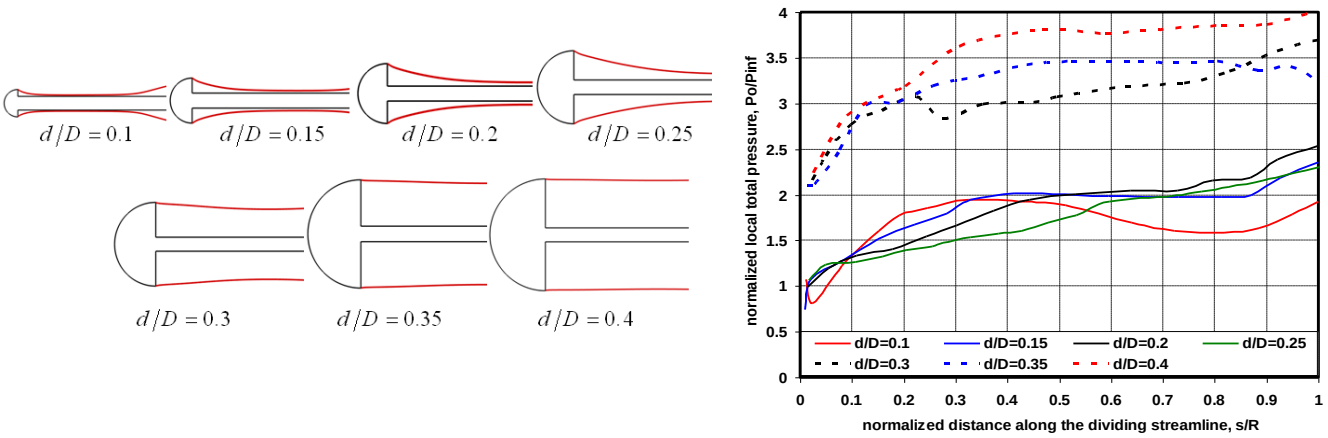

(a) (b)

Figure 8 Variation of (a) the shape and (b) the total pressure along the dividing streamlines downstream of separation in models with $L/D = 2.5$

3. Mechanism of aeroheating reduction and the aerothermal characteristics of aerodisks

Holden [19] showed that value of peak aeroheating at the reattachment point is governed by the "geometry of reattachment". The value of the peak heating increases as the angle between the reattaching shear layer and the normal to the body surface, the reattachment angle, decreases. angle of shear layer impingement (reattachment) with respect to the tangent to the body face. Apart from Holden's study [19], a comprehensive investigation of the mechanism of aeroheating reduction on spiked bodies was not conducted. The authors conducted a study [20] devoted to addressing this phenomenon on the models illustrated in the beginning of this section. The variation of wall temperature along the forebody surface of three models with sharp-pointed spikes is shown in Fig. 9 below. The adiabatic wall temperature is normalized with respect to the adiabatic wall temperature at the stagnation point of the unspiked body in the same freestream conditions, T_{ref} .

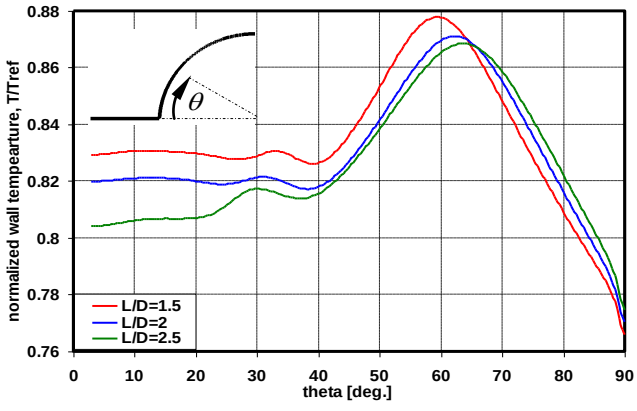

Figure 9 Variation of forebody surface temperature with the spike length

Consistent with Holden [19], the peak aeroheating value depends on the reattachment angle. Here, as the spike length increases, the reattachment point moves towards the forebody shoulder, and the strength of reattachment (expressed in terms of the reattachment angle) decreases. Hence, the peak temperature decreases. This reflects a major difference between pressure and temperature peaks. While the former is created by the reattachment shock wave, the latter is created due to the impingement of the shear layer on the forebody surface. Therefore, the reattachment point can be more accurately located using the peak heating rather than the peak pressure. However, increasing the spike length reduces the wall temperature ahead of the entire body and not only in the reattachment zone. The aeroheating on the forebody surface inside the recirculation zone is explained as follows. Recalling that the aeroheating is directly related to the skin friction (and hence, the velocity gradient) through the Reynolds analogy [21], it is better to first investigate the vortex structure inside the recirculation zone. The recirculation zone incorporates three vortices. The primary one is situated immediately below the shear layer and is initiated by the impingement of the latter on the body surface. A smaller secondary vortex is established below the primary one and a tiny tertiary one is created at the spike root. The primary vortex, which is the largest, increases in size as the spike length increases on the expense of the neighboring vortex. This is illustrated in Fig. 10 whereas Fig. 11 illustrates the variation of skin friction coefficient profile along the forebody with spike length.

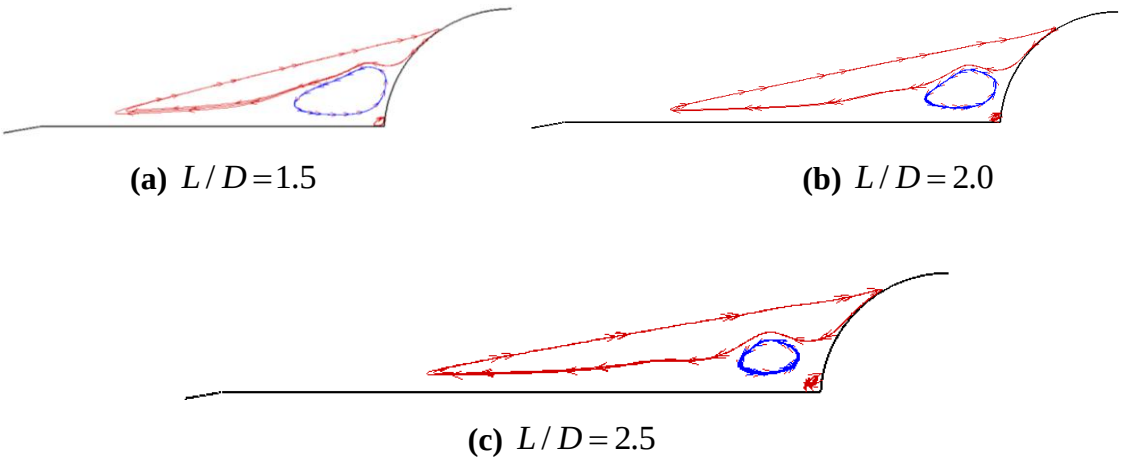

(a) $L/D=1.5$ **(b)** $L/D=2.0$

(c) $L/D=2.5$

Figure 10 Vorticity structure inside the recirculation zone for three models with sharp spike

The flow in the primary and tertiary vortices generates a negative shear stress whereas the flow in the secondary vortex and downstream of reattachment zone generates a positive shear stress. For the short spike, $L/D=1.5$, the velocity gradient at the forebody wall caused by the primary vortex is higher due to the smaller size of the vortex. This causes the aeroheating to increase in the portion of the forebody exposed to the primary vortex. Increasing the spike length yields a more slender effective body. Hence, the velocity gradient and the skin friction of the primary vortex, decreases yielding a lower surface heating to the forebody surface. The mechanism of aeroheating is different in the spiked and unspiked cases. In the unspiked forebody, the flow behind the strong bow shock wave attains significantly high temperature levels which are responsible for the aeroheating of the forebody surface. In contrast, in the spiked forebody, the aeroheating at the reattachment is caused by the impingement of the shear layer on the surface and the consequent vorticity generation.

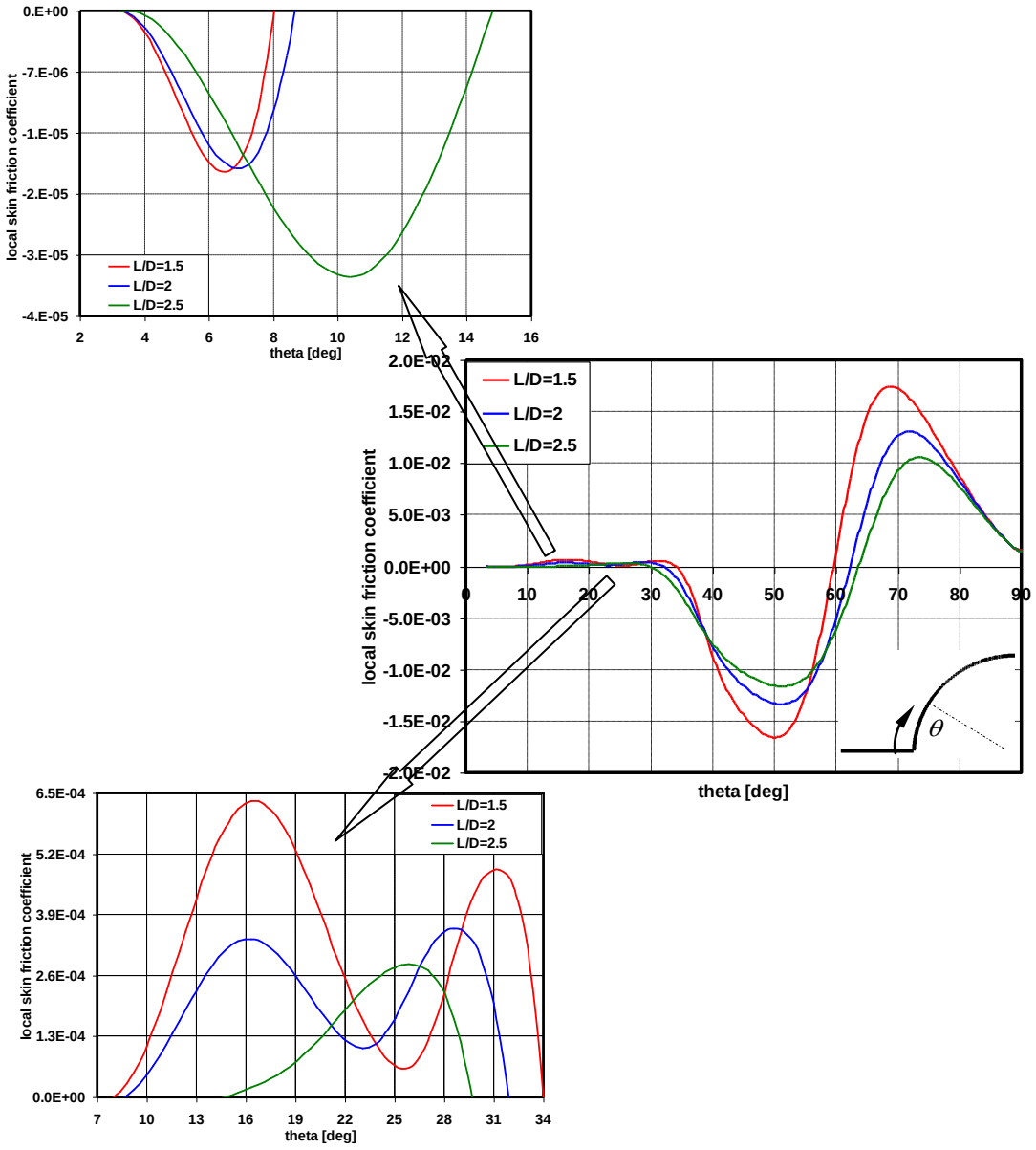

Figure 11 Variation of skin friction coefficient along the forebody with spike length

The variation of adiabatic wall temperature and shear stress on the forebody surface with the aerodisk size are illustrated in Fig. 12 below for models with $L/D=1.5$. The aeroheating increases rather than decreases by replacing the pointed spike tip with a rounded one. This finding is consistent with the experimental measurements of Motoyama et al. [22]. They showed that the total heat flux to the model with a rounded-tip spike exceeded that of the sharp-pointed spike. The impact of the aerodisk size of the reattachment heat flux was not addressed.

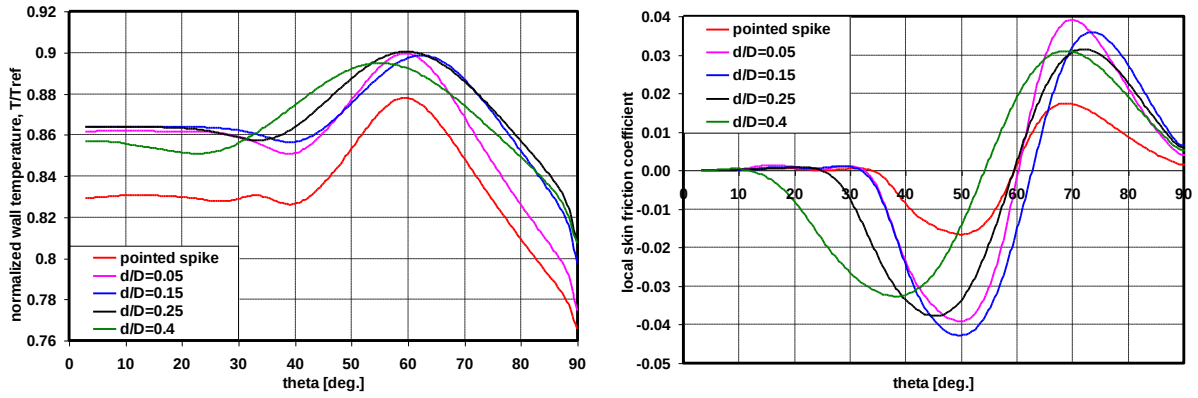

(a) **(b)**

Figure 12 Impact of aerodisk size on the forebody (a) temperature, and (b) skin friction coefficient

As inferred from Fig. 12 above, by increasing the aerodisk size, the levels of aeroheating remain almost the same regardless to the aerodisk size; this trend can be explained as follows. Rounding the spike tip and increasing the aerodisk size increase the shear layer energy in two aspects namely, the large size of the expansion fan ahead of the separation shock and the low inclination of the latter. Consequently, the shear stress in the vicinity of the forebody increases and, hence, the aeroheating increases. Further increasing the aerodisk size causes the shear layer to be more energetic and the primary vortex to be larger. The overall outcome is an insignificant variation in the peak aeroheating at the reattachment point. This trend of forebody surface temperature variation with aerodisk size persists for models with longer spikes [20]. In all cases, spikes and aerodisks yield a reduction in the aeroheating to the entire forebody. They also reduce the peak heating value and shift its location away from the stagnation point which is generally occupied by heat-sensitive instruments such as seekers. However, being exposed to the freestream, the spike tip and aerodisks are expected to encounter excessive aeroheating in place of the forebody. It is thus useful, in practical applications, to be aware of the aeroheating levels in and the possible countermeasures. We can expect that aerodisks are exposed to higher aeroheating levels compared with pointed spikes. In either case, the heating intensity is high since it affects a very small surface area. A special heat-resistant material or a thermal coating (protective shields) can be used in the production of the spike tip/ aerodisk.

4. Impact of the spike and aerodisk on the base drag

It is well established that the spikes reduce the pressure drag on the forebodies of the high-speed vehicles by reducing the local surface pressure. A more forebody pressure drag reduction is gained by using aerodisks. But what is the subsequent impact of using aerodisks on the base drag? The answer to this question was not comprehensively discussed in the literature. Bogdonoff and Vas [23] argued that using a spike would reduce the base pressure. In the experimental investigations [8,7,24], the aerodisk were found to yield less total drag compared with pointed spikes. In these experiments, the drag on the whole model was directly measured using force balances and the individual drag components were not investigated.

To address this aspect, the authors conducted a special numerical experiment [2] involving two models having a hemispherical forebody and the same spike overall length of $L/D=1.5$. Model 1 is equipped with a pointed spike whereas model 2 is equipped with an aerodisk having $d/D=0.15$. The computed pressure and velocity contours for both models are illustrated in the upper and lower halves of Fig. 13a and b, respectively.

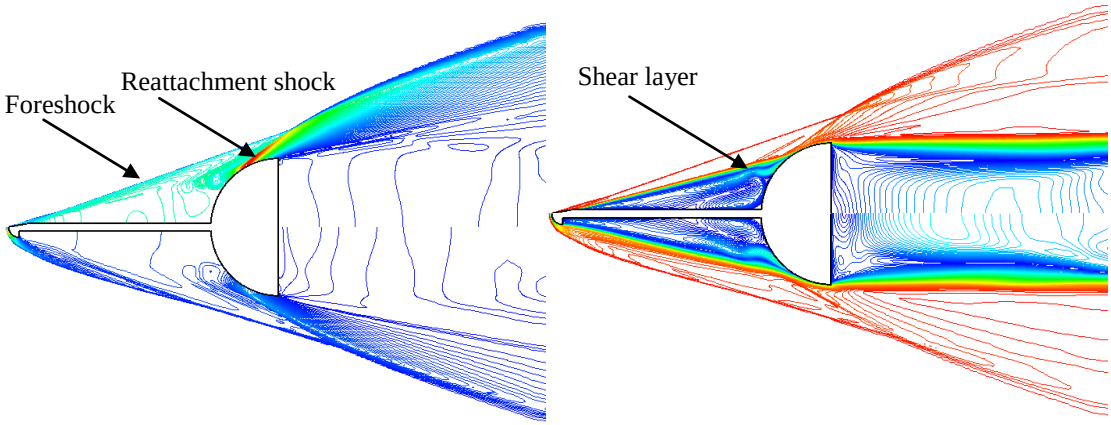

(a) pressure contours **(b) velocity contours**

Figure 13 Flowfield features of the extended computational domain

The pointed spike generates a conical attached foreshock whereas the aerodisk yields a bow detached foreshock. However, as explained before, the flowfield pressure downstream of the foreshock is mainly dictated by the form of the effective body outlined by the dividing streamline. The effective body in case of model 2 is slightly more slender than that of model 1. In both models, the flow separates at the forebody shoulder forming a shear layer that propagates downstream of the forebody base. Downstream of the reattachment shock in both models, the flow expands dictated by the curvature of the forebody shoulder. Since the reattachment shock in model 1 is much stronger, the local pressure at the forebody base is higher. Figures 14a and b illustrate the pressure coefficient profiles along the forebody face and base for both models, respectively. It is clear that, compared with model 2, the pressure is higher in model 1 everywhere along the forebody face and base. This is reflected in the corresponding pressure drag coefficient as shown in Table 1.

Table 1 Components of the pressure drag coefficients for base drag test

	Forebody face	Forebody base	Total pressure drag coefficient
$d/D=0$	0.23164	0.00168	0.2339
$d/D=0.15$	0.1418	0.00444	0.1658

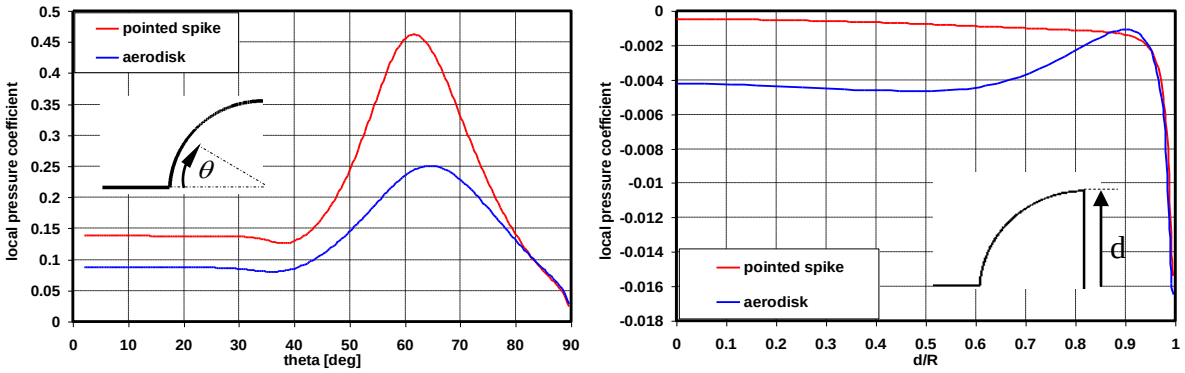

(a) **(b)**

Figure 15 Pressure coefficient profiles along the forebody (a) face, and (b) base

Despite that the aerodisk yields a higher base drag, the drag reduction on the face of the model is more pronounced. The base drag on both models is two orders of magnitude less than that on the models' faces. Overall, the total drag is reduced by replacing the pointed spike with an aerodisk. We would expect that, increasing the aerodisk size has the effect of increasing the base drag but reducing the overall drag.

5. Mechanism of flow instability around spiked hemispherical bodies

The flow instability associated with spiked bodies was thoroughly investigated in many studies. However, these studies mainly focused on models in which flow instability is relatively more pronounced, namely, flat cylindrical and cone cylindrical models. On the other hand, flow instability around spiked hemispherical models gained less attention. Mair [12] and Maull [25] did not record any flow instability associated with such models. However, Crawford [5] indicated signs of shear layer and foreshock "waviness" in his experiments. Yamauchi et al. [9] also reported flow unsteadiness in their own experiments at Mach 2 and 4.5 and supported their experimental findings with numerical analysis. They also reproduced numerically the experiments of Crawford [5]. In all cases, flow instability was claimed to be caused by the unsteady vortices inside the recirculation zone. In his numerical reproduction of Crawford's experiment, Mehta [26] recorded periodic pressure variation on both spike and forebody surfaces, which was argued to indicate self-sustained flow oscillations. Nevertheless, no comprehensive investigation on the occurrence of flow instability around hemisphere cylindrical bodies, its cause, mechanism, and the associated range of model designs has been conducted so far. In the context of their research [2], the authors investigated the flow stability around such bodies; the models mentioned in the beginning of Sec. III.1 are investigated. The majority of these 45 models showed stable flow features. However, for some models the flow was unstable. The impact of the model design on the associated flow stability status in shown in Fig. 16.

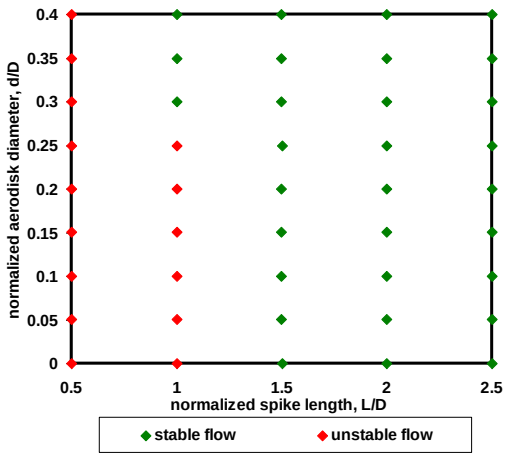

Figure 16 Dependence of flow stability on spike length and aerodisk size

The green and red markers refer to models with stable and unstable flow modes, respectively. Generally, for the specific freestream conditions investigated, the flow around the spiked model can be stable if the spike length exceeds the forebody diameter. More interestingly, increasing the aerodisk size can stabilize the flow. Models with ($L = D$) experience a stable flow if the aerodisk diameter exceeds 25% of the forebody diameter.

The flowfield of a stable flow maintains a fixed pattern that does not change with time. As suggested by Chapman [14], the fundamental criterion of a stable flow is that the dividing

streamline emanating at the separation point is the same dividing streamline stagnating at the reattachment point, Fig. 17a. This only occurs if the energy level of the dividing streamline (in terms of its total pressure) at the reattachment point is sufficiently very close to peak pressure generated by the reattachment shock wave. This pressure balance on both sides of the dividing streamline at reattachment imposes a mass balance. Hence, the dividing streamline keeps a fixed position, and the shape of the effective body (Fig. 17b) remains unchanged. Eventually, the flow field features as well as the associated drag remain unchanged.

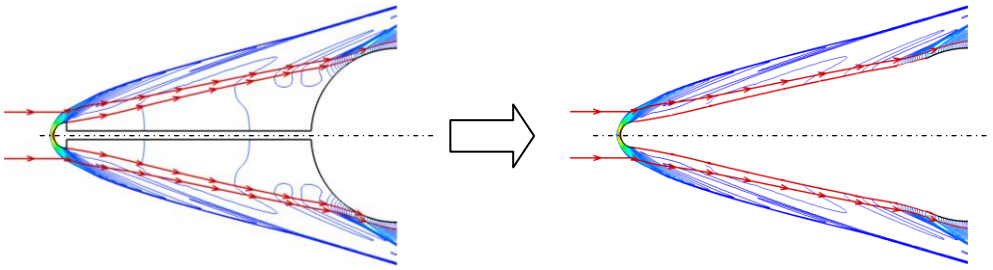

(a) **(b)**

Figure 17 Criteria of the stable flow mode

On the other hand, the flowfield associated with this model continuously changes its pattern with time. The instantaneous static pressure contours around a model experiencing an unstable flow at two different instances (frames) are shown in Fig. 18 a and b, respectively.

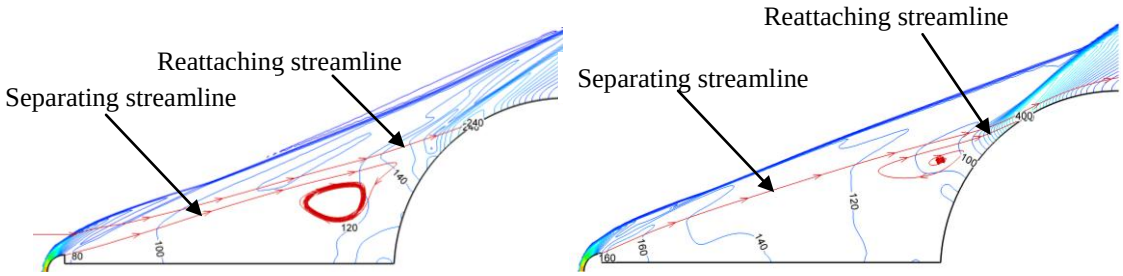

(a) **(b)**

Figure 18 Variation of flowfield and the drag coefficient in the unsteady flow mode

Closely examining the frames below shows that, the streamline emanating at the aerodisk shoulder either reverses into the recirculation zone (frame a) or escapes downstream of the reattachment zone (frame b) and another streamline reattaches on the forebody surface. Since no single streamline links the separation and reattachment points, the term "dividing streamline" is no longer accurate. Feszty et al. [18] introduced the terms "bounding" streamline and "escape" streamline to refer to that emanating from the aerodisk shoulder and that reattaching on the forebody surface, respectively. However, we find it more meaningful to introduce two new terms namely, "separating" and "reattaching", respectively. Depending on the mutual position of the separating and reattaching streamlines, two different situations can be distinguished. In frame (a), the reattaching streamline originates from the farfield and engulfs the separating streamline. The latter then reverses into the recirculation zone. In contrast, in frame (b), the reattaching streamline originates from within the recirculation zone and is engulfed by the separating streamline. The latter manages to escape downstream along the reattachment zone. In either situations, the location and, hence, the strength of the reattachment shock wave are dictated by the stagnation location of the reattaching streamline

(reattachment point). A comprehensive illustration of the mechanism of flow instability and a complete description of its cycle can be found in [10]. They are briefly illustrated below.

At a given instance, the energy level of the separating streamline is such that its total pressure as it approaches the reattachment zone is insufficient to reach the reattachment point. It thus reverses into the recirculation zone and another "more-energetic" streamline emanating from the freestream stagnates on the forebody at the reattachment zone. Such arrangement creates a net mass influx to the recirculation zone causing its inflation. This mass influx energizes the separating streamline such that its total pressure at reattachment gets higher than that required for reattachment. Another "less-energetic" streamline emanating from the recirculation zone stagnates on the forebody at the reattachment zone. Such arrangement creates a net mass outflux from the recirculation zone causing its collapse. This reduces the energy of the separating streamline such that its total pressure at reattachment gets lower than that required for reattachment and the cycle is repeated in a self-sustained manner.

The mechanism of flow instability as explained above is based upon the status of the energy level (in terms of total pressure) of the dividing streamline. To confirm this assumption, the evolution of total pressure along the separating streamline (S, dashed lines) and the reattaching streamline (R, solid lines) in both frame (a, in blue) and (b, in red) are illustrated in Fig. 19. The dash-dot lines indicate the value of peak pressure (P) at the reattachment zone. Clearly, in both situations, the terminal energy level of reattaching streamline is very close to the peak pressure value. The total pressure of the separating streamline in frame (b) is higher than the peak pressure at stagnation. In contrast, the separating streamline in frame (a) possesses a total pressure which is always below the peak pressure value.

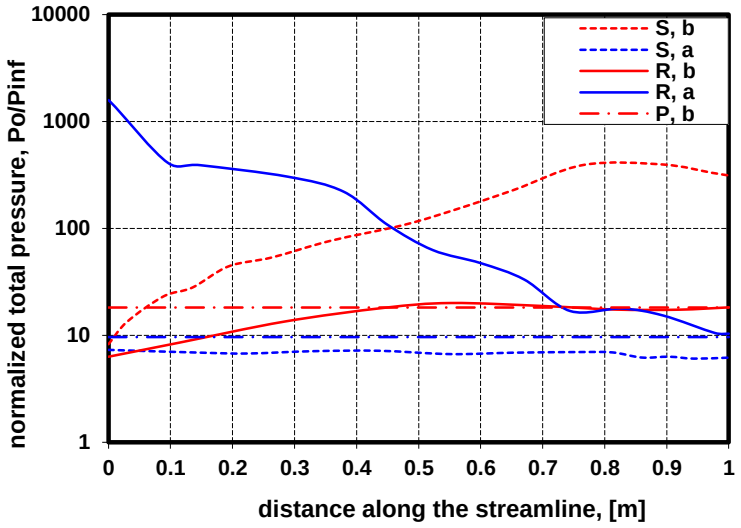

Figure 19 Total pressure of the separating and reattaching streamlines in frames (d) and (i)

An overview of a complete cycle of flow unsteadiness indicates that it falls below the flow oscillation mode type in which both the shear layer and the foreshock perform a lateral flapping-like motion with small amplitude and low frequency. Kenworthy [16] recorded and explained the same characteristics of oscillation flow mode on flat cylindrical bodies. Here, flow instability of the oscillation mode is extended to hemispherical models which were not studies in the previous investigations.

6. Revisiting the assumption of flow axisymmetry at zero incidence

At zero incidence, the flow around the spiked models is assumed by researchers to be axisymmetric even for models experiencing flow unsteadiness. This assumption was confirmed in a number of experimental works [9,27,28] and was adopted in all the previous numerical studies. The validity of this assumption in numerical investigations was explicitly addressed in [9,29-31]. Only Calarese and Hankey [32] showed that, in some cases, there could be a degree of flow asymmetry about the spike axis. In this section, the validity of flow axisymmetry assumption is revisited by highlighting the differences between the axisymmetric and the three-dimensional solutions of the same model. Here, a model having a hemispherical forebody and a pointed spike with $L/D=1.5$ is studied in a full three-dimensional domain. One quarter of the grid used in this investigation is shown in Fig. 20. The grid is designed so as to be clustered and aligned in the location of the shear layer and the foreshock.

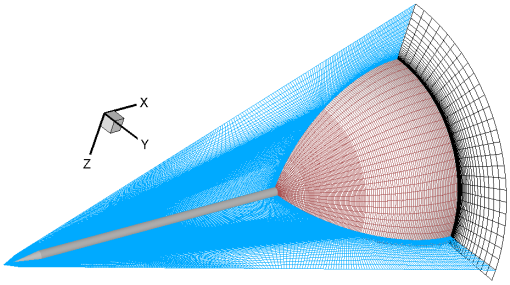

Figure 20 One quarter of the discretised computational domain for the flow axisymmetry investigation

Both solutions gave the same overall performance; the total drag coefficient on the model were found to have the same value. The flowfield features in both solutions are compared in Fig. 21 below. Both the pressure and velocity contours are shown for the axisymmetric domain and the pitch and yaw planes of the 3D domain.

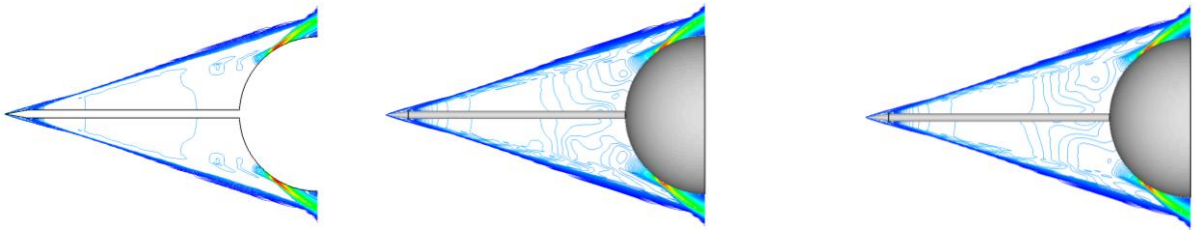

Axisymmetric domain **3D, pitch plane** **3D, yaw plane**

(a) pressure contours

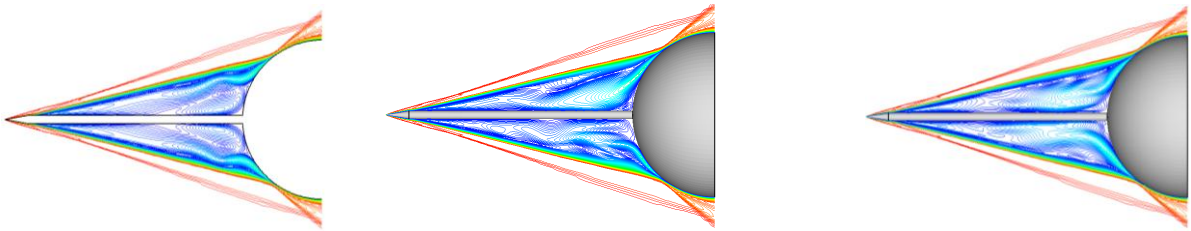

Axisymmetric domain **3D, pitch plane** **3D, yaw plane**

(b) velocity contours

Figure 21 Comparing the flowfield features of the axisymmetric and 3D solutions

Closely examining the above figure indicates that both the axisymmetric and 3D solutions captured nearly identical general flow features. The slopes of the foreshock and the reattachment shock and the location of their intersection are the same. The points of shear layer separation and reattachment and its inclination are also identical in both domains. However, the 3D solution indicates a degree of non-axisymmetry of the flow inside the recirculation zone. To illustrate this, the pressure and velocity contours at different locations along the spike are shown in Fig. 22.

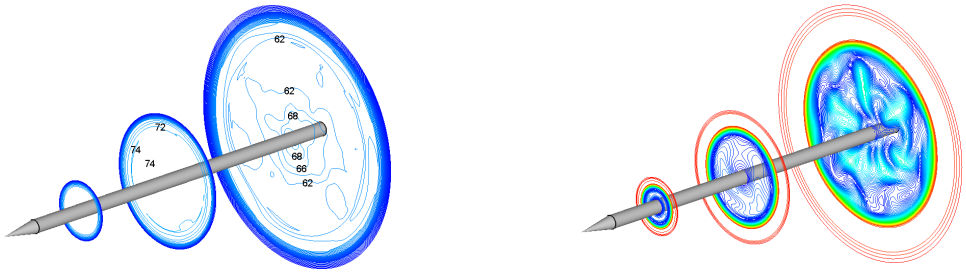

(a) **(b)**

Figure 22 Contours of the (a) pressure, and (b) velocity at different axial locations

The gauge pressure contours are clearly non-circular which yields a circumferential rotation of the flow inside the recirculation zone as inferred from the velocity contours. The level of non-axisymmetry increases as the flow approaches the forebody face. Outside the recirculation zone, the flow is axisymmetric as indicated from the perfectly circular pressure and velocity contours. Since the flow inside the recirculation zone cannot maintain a fixed pattern, the 3D solution is switched to the time-dependent solver. The total drag coefficient as predicted by the time-dependent 3D case was found to vary within 10 drag counts about the mean value. Three check points (corresponding to different time instances) were chosen to investigate the variation in the flowfield structure. Figure 23 illustrates the instantaneous flowfield features at these points.

Apart from the recirculation zone, the flow maintains the same features that do not change with simulation time; it also axisymmetric. Inside the recirculation zone, the flow can not maintain an axisymmetric flow and is, hence, no longer steady. The pressure and velocity contours are non-circular and their patterns change with simulation time. However, since the values of pressure contours are generally low and the variation between contours is insignificant, the resulting drag variation is indistinguishable.

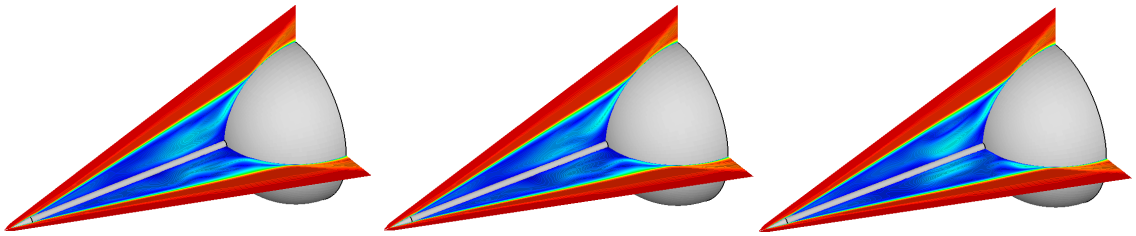

(a) velocity contours on the pitch and yaw planes

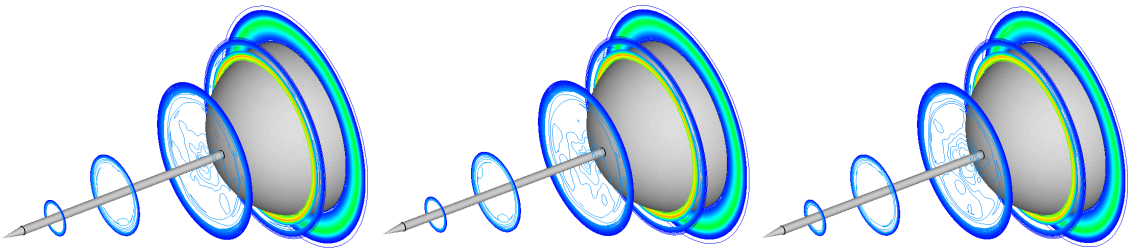

(b) pressure contours on different axial locations

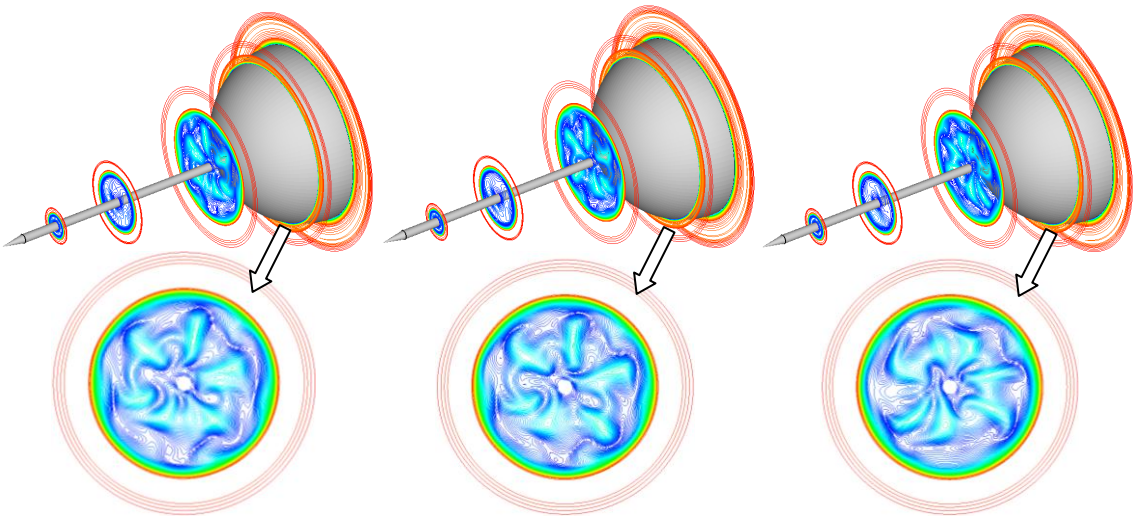

(c) velocity contours at different axial locations

Figure 23 The instantaneous flowfield features at different simulation time instances

B- Forebody Design Optimization of Spiked Hypersonic Vehicles

It is well-known that, under certain flight conditions, the performance of spikes as drag and aeroheating reduction devices varies depending on both the blunt forebody geometry and spike designs [19,33]. It is also proved that the spike's efficiency does not improve monotonically with the spike length [7,34-36] or the aerodisk size [22,37]. The need to optimize the spiked blunt forebody design was explicitly highlighted in the literature [6,7,19,22,37,38]. However, a study dedicated for the design optimization of spiked blunt bodies in high speed regimes was not conducted so far. The study of the authors [39] is dedicated to finding the optimum design(s) of a spiked blunt forebody through a surrogate-assisted, CFD-based, multi-objective, evolutionary optimization. The shape and geometric entities of the spiked forebody to be optimized are illustrated in Fig. 24 whereas the freestream conditions correspond to a flight at an altitude of 60Km with Mach 6 and zero incidence.

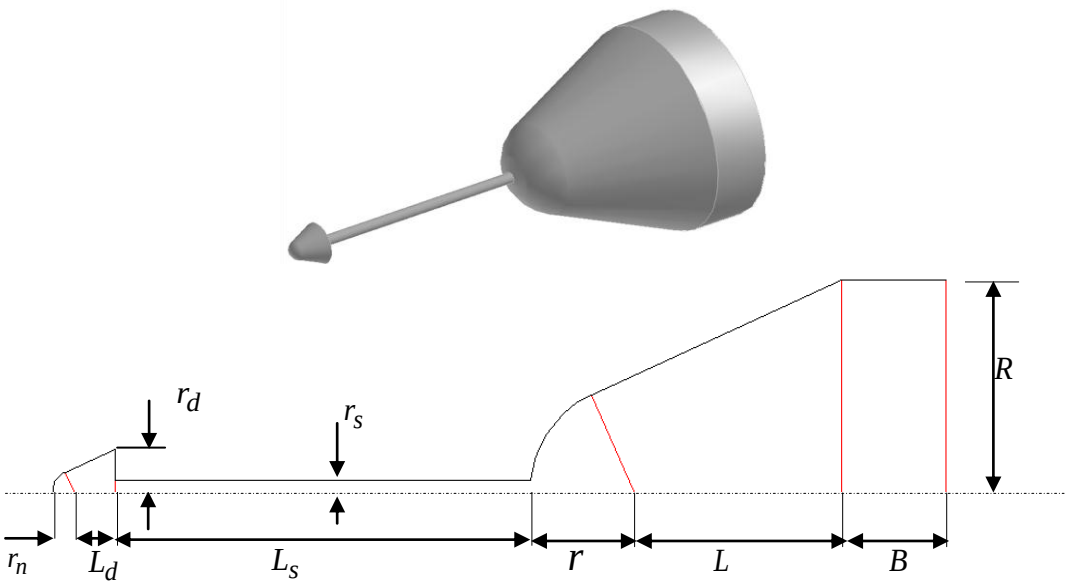

Figure 24 Geometry and design parameters of the spiked blunt forebody to be optimized

Out of the nine geometric entities illustrated in Fig. 24, six are chosen as the important, independent design parameters to be optimized; the bounds of variation of their values are as follows (per unit forebody diameter):
$L = 0.0: 1.0$, $r = 0.02: 0.5$, $L_S = 0.04: 4.0$, $L_d = 0.0: 0.15$, $r_d = 0.02: 1.0$, and $r_n = 0.0: 0.1$

Other geometric entities are given fixed values as follows:

$R = 0.5$, $B = 0.25$, and $r_S = 0.02$

The optimization problem involves two objectives namely, minimum drag and minimum aeroheating. The total drag coefficient (referred to the freestream conditions and the base area of the forebody) is taken as the measure for the drag objective. The peak heat transfer rate to the forebody is taken as a metric for the aeroheating objective. The stability of the flow around the spiked forebody is introduced as constraint for the optimization. The amplitude of variation in the drag coefficient with numerical solution iterations is taken as the metric for the stability constraint. The values of these two objectives and the constraint are taken from the output of the CFD solver. The NSGA-II [40] is taken as the optimizer for this multi-objective constrained problem, the NSGA-II toolbox [41] in Matlab [42] is utilized in this study. Instead of directly coupling the optimizer with the "expensive" flow solver, surrogates are used. To construct the surrogates, a set of 200 training samples is selected from the design space using the space-filling MM-LHD [43] sampling technique. Each sample in the training set resembles a unique design whose objectives and constraint values are taken from the output of the CFD solution. Based on these values, a Kriging surrogate [44] is used to construct a surrogate for each of the objectives and the constraint. The SURROGATES toolbox [45] in Matlab is utilized in this study. The accuracy of the constructed surrogates is assessed using the cross-validation technique [46] and is iteratively improved by adding the so-obtained optimum designs in each iteration to the training samples of the next iteration.

Two optimization problems were considered namely, unconstrained and constrained optimization problems. In the first one, the stability constraint is overlooked whereas in the second one the stability constraint is considered. The impact of population size and

generations number is tested and the solution is found to converge to the Pareto surface after 1000 generations using 1000 individuals. The locations of the Pareto optimal solutions in the objective space, the Pareto fronts, for both optimization problems are illustrated in Fig. 25.

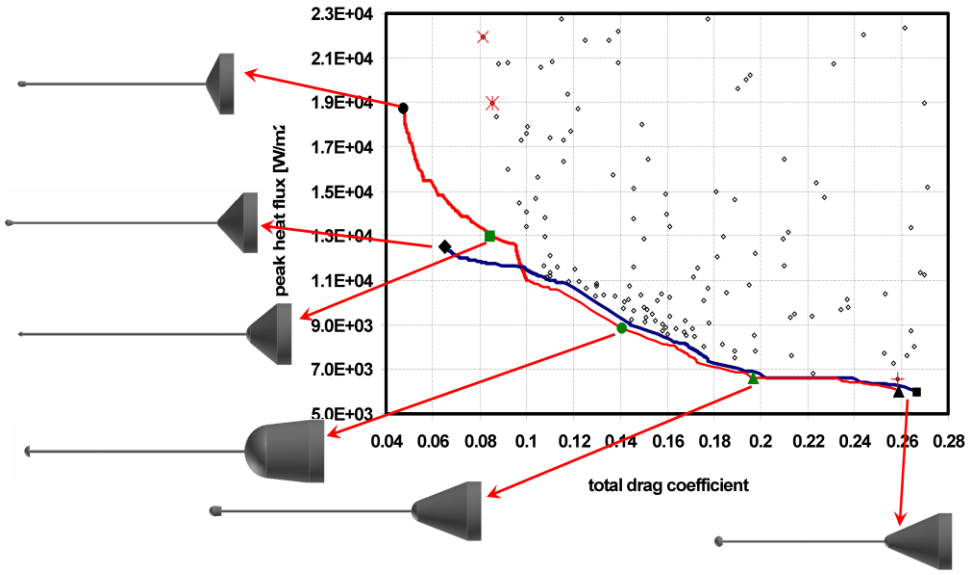

Figure 25 Pareto front of the full-scale optimization problem

The blue and red lines indicate the Pareto front for the constrained and unconstrained optimization problems, respectively. Compared with the original training samples, the Pareto optimal designs of both problems show a considerable performance improvement in both objectives. The evolution of the design of forebody, spike, and aerodisk along both the constrained and unconstrained Pareto fronts is also illustrated in Fig. 25. Generally, a slender forebody with a small nose roundness is preferred for minimum aeroheating. On the other hand, a blunt forebody face is advantageous as far as drag reduction is concerned. increasing the flatness of the forebody face would invoke flow instability. Between these two extremes, a variety of compromise designs can be found; selecting one of them is left to the decision maker according to the importance of the design objectives. More details about the features of the training samples and the optimum designs can be found in [39].

III. Conclusions and Future Perspective

The rich research area of the spiked bodies aerothermodynamics has attracted the interest of the researchers over the years. In the first part of this study [1], these efforts have been surveyed. In this part, the humble participations of the authors are summarized. There are many studies are yet to be conducted in this field. To name a few, the concept of the pivoting spike [47], the effect of aerodisk rotation [48]. In practical applications, the bending and vibration of spikes [14] need more investigation. Similarly, the role of rounding the shoulder of a flat-faced spiked body in stabilizing the flow [49] invokes more studies. In addition, a comparison between spikes and the similar drag reduction devices, e.g., forward-facing jets, may be held. A hybrid device can be proposed. Moreover, the nature of flow asymmetry inside the recirculation zone requires more investigation. Finally, design optimization studies at different flight regimes can be conducted. The design optimization can be further extended to include other design considerations such as volumetric requirements, spike bending and vibration either as objectives, constraints, or even in a multidisciplinary optimization.

References

[1] Ahmed, M. Y. M. and Qin N., "Spiked Bodies Aerothermodynamics: Part I" Proceedings of the 14th International Conference on Aerospace Sciences and Aviation Technology, Cairo, Egypt, May 2011.

[2] Ahmed M. Y. M., "Aerothermodynamic Design Optimization of Spiked Hypersonic Vehicles," Ph.D. Dissertation, Department of Mechanical Engineering, University of Sheffield, Sheffield, U.K., 2010.

[3] Fluent 6.3 User Guide, Fluent Inc., Lebanon, NH 03766 , USA.

[4] Gambit 2.4 User Guide, Fluent Inc., Lebanon, NH 03766 , USA.

[5] Crawford, D. H. "Investigation of the Flow over a Spiked-Nose Hemisphere-Cylinder," NASA TN-D-118, Dec.1959

[6] Gnemmi, P., Srulijes, J. and Roussel, K., "Flowfield around Spike-Tipped Bodies for High Attack Angles at Mach 4.5," Journal of Spacecraft and Rockets, Vol. 40, No. 5, 2003, pp. 622- 631

[7] Kalimuthu, R., Mehta, R. C., and Rathakrishnan, E., "Experimental Investigation on Spiked Body in Hypersonic Flow," The Aeronautical Journal, Vol. 112, No. 1136, 2008, pp. 593- 598

[8] Menezes, V., Saravanan, S., Jagadeesh, G., and Reddy, K. P. J., "Experimental Investigations of Hypersonic Flow over Highly Blunted Cones with Aerospikes," AIAA Journal, Vol. 41, No. 10, 2003, pp. 1955- 1966

[9] Yamauchi, M., Fujii, K., and Higashino, F., "Numerical Investigation of Supersonic Flows Around a Spiked Blunt Body," Journal of Spacecraft and Rockets, Vol. 32, No. 1, 1995, pp. 32 -42

[10] Ahmed, M. and Qin, N., "Drag Reduction Using Aerodisks for Hypersonic Hemispherical Bodies," Journal of Spacecraft and Rockets, Vol. 47, No.1, 2010, pp. 62-80.

[11] Alexander, S. R., "Results of Tests to Determine the Effect of a Conical Windshield on the Drag of a Bluff Body at Supersonic Speeds," NACA RM L6K08a, January, 1947.

[12] Mair, W. A. "Experiments on Separation of Boundary Layers on Probes in front of Blunt-Nosed Bodies in a Supersonic Air Stream," Philosophy Magazine, Ser.7, Vol.43, No. 243, July 1952, pp. 695-716

[13] D'Humieres, G. and Stollery, J. L., "Drag Reduction on a Spiked Body at Hypersonic Speeds," The aeronautical Journal, Vol. 114, No. 1152, 2010, pp. 113-119

[14] Chapman, D. R., Kuehn, D. M., and Larson, H. K., "Investigation of Separated Flows in Supersonic and Subsonic Streams with Emphasis on the Effect of Transition," NACA TR 1356, 1957

[15] Wood, C. J., "Hypersonic Flow over Spiked Cones," Journal of Fluid Mechanics, Vol. 12, Pt. 4, 1961, pp. 614–624.

[16] Kenworthy, M., "A Study of Unsteady Axisymmetric Separation in High Speed Flows," Ph.D. Dissertation, Dept. of Aerospace and Ocean Engineering, Virginia Polytechnic Inst. And State Univ., Blacksburg, VA., 1978.

[17] "Equations, Tables, and Charts for Compressible Flow," NACA TR 1135, 1953.

[18] Feszty, D., Badcock, K. and Richards, B., "Driving Mechanisms of High-Speed Unsteady Spiked Body Flows, Part2: Oscillation Mode," AIAA Journal, Vol. 42, No. 1, 2004, pp. 107- 113

[19] Holden, M., "Experimental Studies of Separated Flows at Hypersonic Speeds. Part I-Separated Flows over Axisymmetric Spiked Bodies," AIAA Journal, Vol. 4, No. 4, 1966, pp. 591-599.

[20] Ahmed, M. and Qin, N., "Numerical Investigation of Aeroheating Characteristics of Spiked Blunt Bodies at Mach 6 Flight Conditions," The Aeronautical Journal, In press.
[21] Anderson, J.D. Fundamentals of Aerodynamics, Fourth Edition, McGraw-Hill, 2007.
[22] Motoyama, N., Mihara, K., Miyajima, R., Watanuki, T., and Kubota, H., "Thermal Protection and Drag Reduction with Use of Spike in Hypersonic Flow," AIAA paper 2001-1828, 2001
[23] Bogdonoff , S. M. and Vas , I. E., "Preliminary Investigations of Spiked Bodies at Hypersonic Speeds," Journal of the Aerospace Sciences, Vol. 26, No. 2, 1959, pp. 65-74
[24] Milicev, S. S. and Pavlovic, M. D., "Influence of Spike Shape at Supersonic Flow Past Blunt-Nosed Bodies: Experimental Study," AIAA Journal, Vol. 40, No. 5, 2001, pp. 1018- 1020
[25] Maull, D. J. "Hypersonic Flow over Axially Symmetric Spiked Bodies," Journal of Fluid Mechanics, Vol. 8, P.4, 1960, pp. 584-592
[26] Mehta, R. C., "Numerical Analysis of Pressure Oscillations over Axisymmetric Spiked Blunt Bodies at Mach 6.8," Shock Waves, Vol. 11, No. 3, 2002, pp. 431-440
[27] Heubner, L. D. Mitchell, A. M. and Boudreaux, E. J., "Experimental Results on the Feasibility of an Aerospike for Hypersonic Missiles", AIAA paper, 95-0737, Jan.1995.
[28] Guenther, R. A. and Reding, J. P., "Fluctuating Pressure Environment of a Drag Reduction Spike," Journal of Spacecraft and Rockets, Vol. 14, No. 12, 1977, pp. 705 - 710
[29] Srinivasan, G. R., and Chamberlain, R. R., "Drag Reduction of Spiked Missile by Heat Addition," AIAA paper 2004-4714, 2004
[30] Feszty, D., Badcock, K., Richards, B., and Woodgate, M., "Numerical Simulation of a Pulsating Flow Arising over an Axisymmetric Spiked Blunt Body at Mach 2.21 and Mach 6.00," Shock Waves, Vol. 10, No. 5, 2000, pp. 323-331
[31] Feszty, D., Badcock, K. and Richards, B., "Numerical Simulation of the Hysteresis Phenomenon in High-Speed Spiked Body Flows," AIAA paper 2000-0141, 2000.
[32] Calarese, W. and Hankey, W., "Modes of Shock-Wave Oscillations on Spike-Tipped Bodies," AIAA Journal, Vol. 23, No. 2, 1985, pp. 185-192.
[33] Antonov, A. N., and Grestov, V. K., "Unsteady Separated Supersonic Flow over Pointed and Spiked Bodies," Fluid Dynamics, Vol. 9, No. 4,1974.pp. 578- 582.
[34] Stalder, J. R. and Nielson, H. V., "Heat Transfer from a Hemisphere Cylinder Equipped with Flow Separation Spikes," NACA TN 3287, Sept. 1954.
[35] Moeckel, W. E., " Flow Separation Ahead of a Blunt Axially Symmetric Body at Mach Numbers 1.76 to 2.10," NACA RM E51I25, 1951
[36] Hermach, C. A., Kraus, K., and Reller, J. O., " Reduction in Temperature-Recovery Factor Associated with Pulsating Flows Generated by Spike-Nosed Cylinders at a Mach Number of 3.50," NACA RM A56L05, March, 1957.
[37] Jones, J. J., "Experimental Drag Coefficients of Round Noses with Conical Windshields at Mach Number 2.72," NACA RM L55E10, June, 1955.
[38] Jagadeesh, G., Viren, M., Reddy, K. P. J., Hashimoto, T., Sun, M., and Takayama, K., "Hypersonic Buzz Phenomenon in the Spiked Blunt Cones," AIAA paper 2003-284, 2003.
[39] Ahmed, M. and Qin, N., "Surrogate-Based Multi-Objective Aerothermodynamic Design Optimization of Hypersonic Spiked Bodies," AIAA Journal, under revision.
[40] Deb, K., Pratap, A., Agarwal, S., and Meyarivan, T., "A fast and elitist multiobjective genetic algorithm: NSGA-II," IEEE Transactions on Evolutionary Computation, Vol. 6, No.2, 2002, pp. 182–197
[41] NSGA-II toolbox for Matlab user guide, http://www.mathworks.com /matlabcentral/fileexchange/10429-nsga-ii-a-multi-objective-optimization-algorithm, cited Jan 2010

[42] Matlab 7 release 14 User Guide, The Mathworks Inc., USA
[43] Morris, M. D. and Mitchell, T. J. "Exploratory Designs for Computational Experiments," Journal of Statistical Planning and Inference, Vol. 43, 1995, pp.381-402
[44] Sacks, J., Welch, W. J., Mitchell, T. J., and Wynn, H. P., "Design and Analysis of Computer Experiments," Statistical Science, Vol. 4, No. 4, 1989, pp. 409-423
[45] Viana, F. A. C., "SURROGATES Toolbox User's Guide," http://fchegury.googlepages.com, Cited, Dec. 2009.
[46] Queipo, N. V., Haftka, R. T., Shyy, W., Goel, T., Vaidyanathan, R., and Tucker, K., "Surrogate-based Analysis and Optimization," Progress in Aerospace Sciences, Vol. 41, 2005, pp. 1-28.
[47] Schulein, E., "Wave drag reduction concept for blunt bodies at high angles of attack," Shock waves 1, Springer Berlin Heidelberg, 2009, pp. 1315-1320
[48] Khlebnikov, V. S., "Effect of Unsteady Disturbances on the Flow in a Forward Separation Zone," Fluid Dynamics, Vol. 27, No. 2, 1992, pp. 294- 297.
[49] Reding, J. P., Guenther, R. A., and Richter, B. J., "Unsteady Aerodynamic Considerations in the Design of a Drag-Reduction Spike," Journal of Spacecraft and Rockets, Vol. 14, No. 1, 1977, pp. 54- 60.